2020-01-1225 Published 14 Apr 2020

Enhancement of Longitudinal Energy Absorption Efficiency in FMVSS 301

Atsushi Hasegawa, Takayuki Fujii, and Norikazu Matsuura Honda R & D

Tomohiro Shimizu Benteler Automotive Corp.

Citation: Hasegawa, A., Fujii, T., Matsuura, N., and Shimizu, T., "Enhancement of Longitudinal Energy Absorption Efficiency in FMVSS 301," SAE Technical Paper 2020-01-1225, 2020, doi:10.4271/2020-01-1225.

Abstract

While active safety has become a focus of attention, passive safety protocols are still being updated, and evaluation standards are becoming stringent worldwide. This paper focused on FMVSS 301, the North American regulation for rear impacts. Due to an offset impact with deformable barrier, it is challenging to control bending modes of rear frames. Furthermore, there is a considerable difference in load paths to the left and right frames, and the amount of bending deformation experienced by the frame on the non-collision-side, which does not directly contact with the barrier, is low. The purpose of this research was to enhance rear-frame energy absorption efficiency in such collisions. To achieve this goal, this research focused on enhancement of deformation mode of the rear frames, and also minimizing the difference in their input loads. For the enhancement of deformation mode, the number and arrangement of collapse points were optimized, and multi-stage bending mode with a high level of energy absorption efficiency was achieved. A partial softening was applied to create an initialization point of bending deformation. In order to reduce the difference in load paths, the length of the central flat section of the bumper beam was set such that the area of impact with the barrier would be symmetrical on both left and right sides. To maintain clearance between the barrier and the bumper beam-end on the collision side for as long as possible, geometrical beam parameters such as bending angles of the beam were also optimized. A stretch bending method was applied for the manufacturing of a prototype beam. This increased the amount of energy absorbed by the frame on the non-collision-side. Impact tests conducted using drop tower tests, which satisfy geometric specifications for mass-production, verified that this approach increased rear-frame energy absorption efficiency by 220%.

Introduction

In recent years, with advances in the performance of devices such as cameras and sensors, active safety technologies that seek to help prevent accidents before they occur are attracting attention. At the same time, protocols in the area of passive safety technologies, which provide safety standards in the event of a collision, are still continuously updated. Particularly in North America, the standards for evaluation in collision test protocols are more stringent than those in other regions.

This research focused on FMVSS 301 (Termed "301" below) [1], which is a requirement for rear collisions safety. Requirements related to rear collisions differ by region, and for North America, 301 specifies an offset impact with a deformable barrier. Due to the offset condition, the frame that directly impacts the barrier (termed "the collision-side frame" below) is required to absorb higher energy during the crash, while the frame on the opposite side (termed "the non-collision-side frame" below) absorbs lower energy levels.

In addition, the deformable barrier generates load input to the vehicle body from various directions during a crash, and this makes it challenging for the body frame to absorb higher energy, especially for frames of 500 mm or longer, which are used in sedan-type vehicles. Moreover, because the collision speed of 80 km/h specified by 301 is at least 30 km/h higher than the speeds employed in rigid barrier protocols, the energy that it is necessary for the vehicle to absorb is approximately three times greater than it is in regions other than North America.

However, factors such as compatibility[2] in car-to-car collisions, and door beam and seat load paths[3] in side collisions[4], have formed the central focus of research on vehicle body configurations, and there has been little research with a focus on North American rear-end collision protocols. With regard to rear bumper beams, a variety of research [5] [6] has been conducted on materials, including application of steel, aluminum and plastics, but the mainstream of research tends to focus on substitution of materials and low-speed collisions. Research in the area of the rear frame focuses exclusively on the application of high-tensile steels including hot-stamped materials [7, 8], λ materials in which a fracture is suppressed[9], tailored blank manufacturing method[10] and partial softening manufacturing method. It is predicted that increases in vehicle weight will gain pace in the future with the equipment of sensors for active safety and the high-capacity batteries for electric vehicles. In addition, it is important to respond to

demands to increase fuel efficiency by reducing vehicle weight while also satisfying evolving safety standards.

Considering this background, the research used a mass-production sedan as a base vehicle and sought to realize a new configuration able to reduce vehicle weight while also increasing energy absorption efficiency in 301. The research focused mainly on a rear-frame configuration that would realize a high level of energy absorption, and a rear bumper beam that would reduce the difference in the load input between the left and right rear-frames during an offset collision. For the rear frame, studies were conducted to determine the position of bending points for deformation. For the rear bumper, the external outline geometry was investigated. Unit evaluations were conducted for each part using simulations, and performance was finally evaluated in drop tower tests on a prototype that incorporated the new configurations.

Investigation of Rear Frame

Figure 1 shows a rear part of a body structure, seen from the bottom of the vehicle. The rear frame is a pair of left and right framework segments and is positioned to connect the front floor to the rear bumper beam. Suspension parts such as the subframe are attached to the rear frame, and the frame is not prone to deformation in these sections. Because of this, a length of between 500 and 700 mm behind the subframe mounting points is the main area for energy absorption in sedan-class vehicles. The cross-section size of the frame is restricted by trunk capacity, and also by adjacent parts such as silencers or spare tire. Given this, 90 x 90 mm is the common size for the cross-section of a rear frame. Additionally, as mentioned in the introduction, it is not easy to realize a high level of stable energy absorption by means of axial crushing in a rear frame of 500 mm or longer in length. Some mass-production vehicles employ soft zones (termed "SZ" below) positioned at equal intervals, which has a proven record in controlling bending modes. However, as Fig. 1(b) shows, with uniform positioning, there is a deviation from the axis of the frame when it deforms (black circled area shown in Fig. 1(b)), and the amount of deformation in the Y-axis is high. Because of this, there is minimal deformation in the hard zones (termed "HZ" below) between each bending point, and the greater part of the energy is absorbed by the SZ. Compared to axial crushing in which the entire rear-frame deforms, energy absorption and average load are low.

Design Concept of Rear Frame

The concept behind the research under discussion was to realize control of a multi-stage bending mode involving more than three points on the rear frame, as shown in Fig. 2, thereby bringing the level of energy absorption close to that of axial crushing deformation. With position and number of the SZ as the design parameters, the following hypotheses were established and tested.

FIGURE 1 Frame deformation mode of conventional vehicle

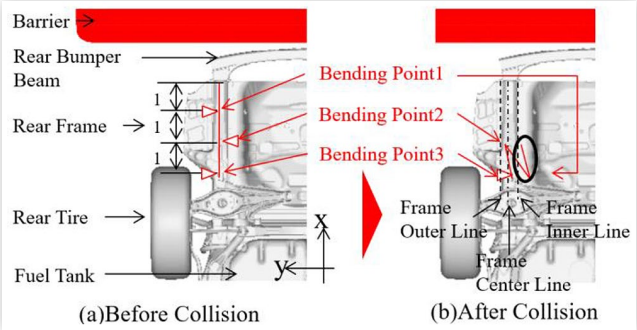

FIGURE 2 Frame deformation mode of new concept

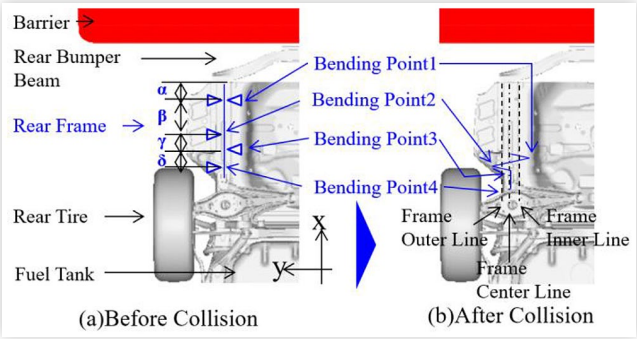

Hypothesis 1): Increasing the number of the SZ would increase the level of energy absorption;

Hypothesis 2): Non-uniform positioning of the SZ would induce deformation that passes through the axis of the frame. This would increase the level of energy absorption by the HZ. If α: β: γ: φ in Fig. 2 were positioned in a 1:2:1:1 ratio, the level of energy absorption would be the highest, because geometrically, deformation would pass through the axis of the frame.

Hypothesis 3): Positioning the SZ at the furthermost rear-end of the vehicle body across the entire cross-section would initiate crushing and would increase the level of energy absorption.

Analysis of Soft Zones

Figure 3 shows the FEM model employed for the investigation of the rear-frame deformation mode. For the study, a sedan was used as the base vehicle and the size of the rear frame was set at a length of 600 mm and a cross-section of 90 x 90 mm. Hot-stamped materials were employed for the rear frame, and yield strength equivalent to 590 MPa steel was allocated to the SZ, which are shown as yellow. The size of the SZ was 45 mm in the X direction, 40 mm in the Y direction, and 90 mm in the Z direction, with 30 mm transition zones (termed "TZ" below) set between HZ and SZ. Because the length of a sedan rear-frame varies from 500 to about 700 mm depending on the model, a maximum of four SZs was set as the upper limit in order to keep feasibility for shorter rear frames such as 500 mm. The bending initiation points were positioned in a zigzag arrangement to help ensure that the

FIGURE 3 FEM model of simplified rear frame for initial investigation

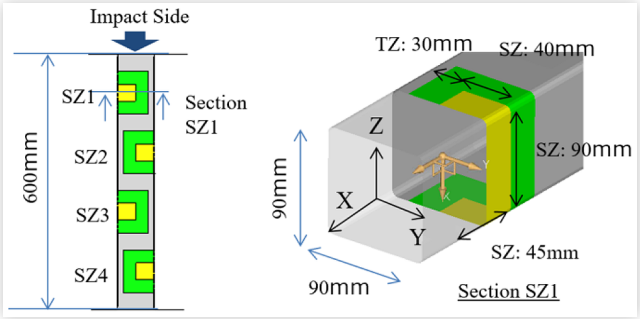

points were not concentrated on one side of the frame. Simulations were conducted for cases of one through four SZs including the non-uniform positioning. In addition, the level of energy absorption was compared with the case of axial crushing of a uniform 590 MPa steel to investigate the validity of the hypothesis. A list of analyses based on position and number of the SZ is shown in Table 1.

Simulation Results of Soft Zones Analysis

Figure 4 shows the simulation results. The horizontal axis shows the sum of energy absorption in the SZ and TZ sections, and the vertical axis shows the total energy absorption by the frame. Red plots show results for one SZ, green for two, purple for three, and blue for four. Points I to IV in Fig. 4 show results for SZ positioned at constant intervals. The relationship between the number of SZs and the level of energy absorption proposed in Hypothesis 1 will be discussed first. The results show that as the number of SZs increase, the energy absorbed by the SZ and TZ increases, and as a result, the total energy absorption increases. While maximum energy absorption for cases of three or fewer SZ was 17 kJ, among cases of four SZs, energy absorption for the models achieving the highest level of energy absorption was more than 15% higher. They are noted as A, B, and C in Fig. 5.

As a next step, the positioning of the SZ considered in Hypothesis 2 was investigated. Among the results for each number of SZ, I to IV were basically the median values of energy absorption. The results show that while there were cases in which energy absorption increased with a non-uniform arrangement of SZ, as per the hypothesis, there were also cases

FIGURE 4 Results of energy absorption at SZ and TZ against total EA

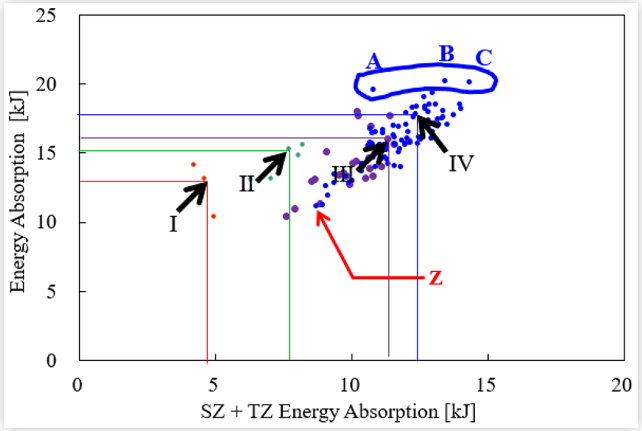

FIGURE 5 Deformation mode of rear frame for models B, IV, and Z

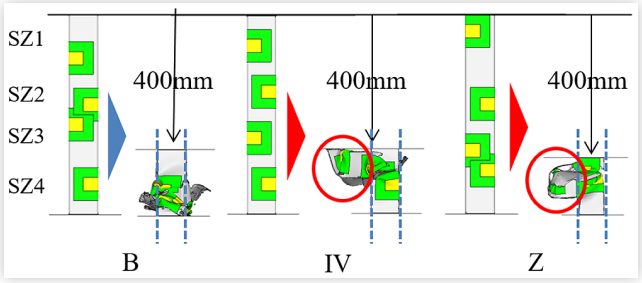

in which it decreased. Factors that influence the energy absorption were considered based on the deformation mode. Figure 5 shows the frame deformation modes for models B and Z, which respectively display the highest and lowest levels of energy absorption for four SZs, and for IV, a result for a uniform arrangement of SZ. As the red circled areas indicate, models IV and Z show deformation that deviates from the axis of the frame in the orthogonal direction. As in the case of a mass-production frame, this is because the sections that deviate from the axis are not crushable. It is considered that this is the reason that energy absorption decreased. Additionally, model A shows the result for positioning of SZ with the interval ratio 1:2:1:1. The difference between the total energy absorption for A and B was slight at 0.6 kJ. Figure 6

TABLE 1 Position and number of soft zones used for simulation

		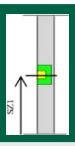	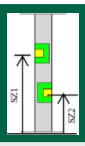	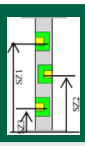	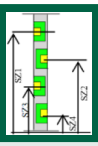
Number of SZ		1	2	3	4
SZ Position	SZ1	300,450,150	300,400,500	475,412,537,	470,510,550
	SZ2		100,200,300	237,300,362	330,370,410,
	SZ3			62,125,187	190,230,270
	SZ4				50,90,130

compares results of energy absorption at HZ for models A, B, C and IV. Energy absorption at HZ is the highest for model A, indicating the validity of Hypothesis 2.

Investigation of Rear-end Soft Zone

Hypothesis 3 was investigated in relation to models A, B, and C, which displayed the highest energy absorption performance. Simulations were conducted under conditions in which SZ1, was enlarged across the entire frame cross-section, as shown in Fig. 7. Following this change, the models were respectively renamed A', B', and C'.

Figure 8 shows changes in energy absorption performance. Energy absorption for model A' increased by approximately 15%, the greatest increase among the three cases examined. Figure 9 shows the deformation process for model A'. It can be seen that SZ1 is crushed, followed by bending at SZ2, 3, and 4 in stages. This deformation mode conforms to the concept. The change in energy absorption for model C' was minimal, but it decreased by approximately 20% for model B'. Figure 10 shows the change in deformation mode before and after the modification of models A and B. In model B', the introduction of the crushing of SZ1 disrupted the balance of deformation, increasing the level of deviation from the axis. This change in deformation mode is considered as the cause of the decline in energy absorption. Figure 11 compares model A', an axial crushing model with uniform 590 MPa material characteristics, and III, which is equivalent to a mass-production vehicle, wherein (a) shows energy absorption, (b) shows average load, and (c) shows the load-stroke characteristic. Model A' produced results for energy absorption and average load equivalent to or higher than the results for the axial crushing case. The load-stroke characteristic was also close to the crushing case, with minimal decline in the load.

Based on the results discussed above, it can be considered that the multi-stage bending control proposed in the research hypotheses realized a level of energy absorption close to that of an axial crushing deformation mode.

FIGURE 6 Energy absorption at HZ for models IV, A, B, and C

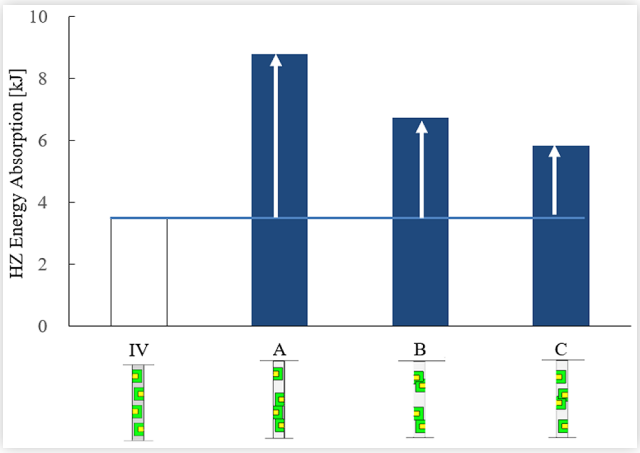

FIGURE 7 Modification of SZ1 with models A, B, and C

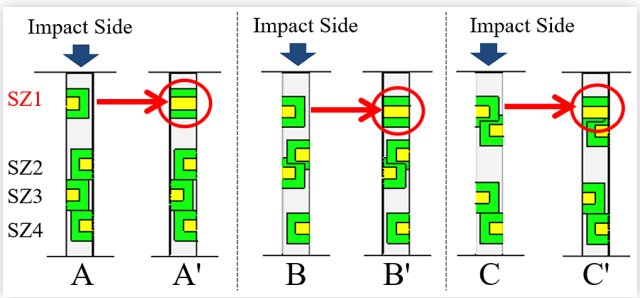

FIGURE 8 Changes in energy absorption before and after modification

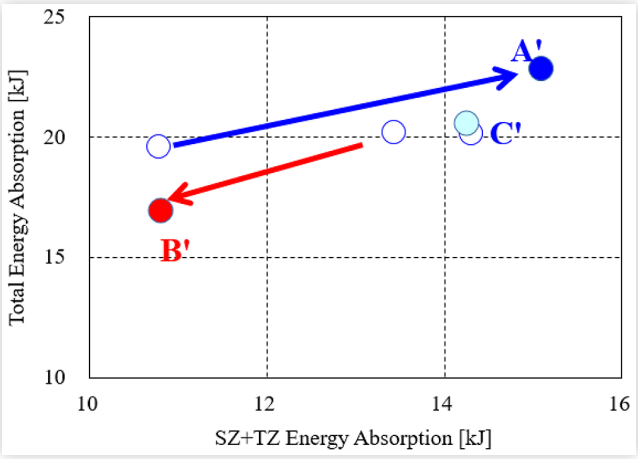

FIGURE 9 Deformation steps of model A' from 0 to 400 mm

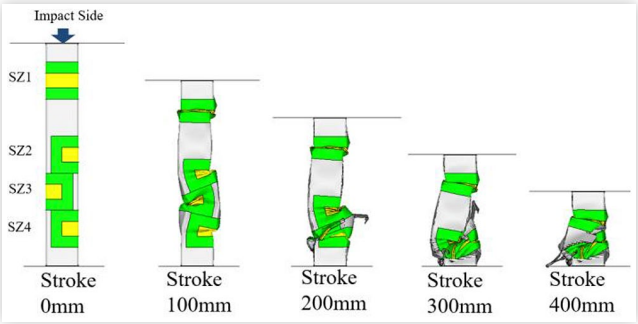

FIGURE 10 Comparison of bending mode before and after modification

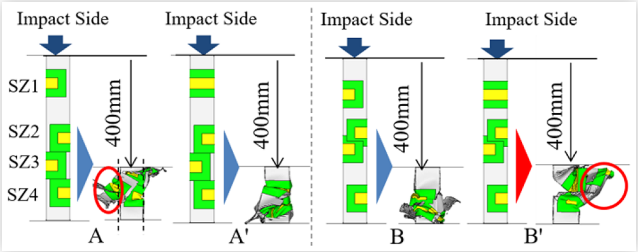

FIGURE 11 Comparison of model A' with axial crush and mass-production models

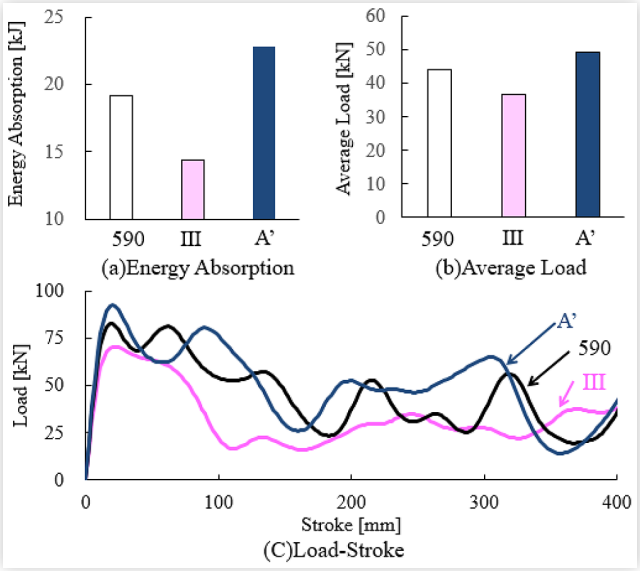

Investigation of Rear Bumper Beam

The rear bumper beam is a structural component that connects the left and right rear-frames, with steel or aluminum commonly used. Figure 12 shows a schematic diagram of the load paths with the bumper beam of mass-production model in 301. F_{mdb} represents the distributed load applied from the barrier to the beam, F_{xc} is the load input from the bumper beam into the collision-side frame, and F_{xnc} is the load applied to the non-collision-side frame. As shown in Figure 12, the barrier is deformed along the outline shape of the bumper beam and this leads to the difference in the load distributed to the two frames. As a result, energy absorption on the non-collision-side of the frame is low.

Design Concept of Bumper Beam

Figure 13 shows the basic concept to achieve symmetrical load input to the two frames. With this concept, energy absorption on the non-collision-side frame is expected to increase. For this research, the following two hypotheses were formulated based on the beam design parameters and vehicle design space.

Hypothesis 1) By keeping the distributed load input F_{mdb} symmetrical with respect to the center of the vehicle at the initial stage of the crash, the load distributed to the two rear-frames would be kept equivalent. To do so, a flat section at the center of the bumper beam should have a certain length such that the contact area with the barrier is kept symmetrical.

Hypothesis 2) To keep the contact area during a crash symmetrical, a clearance should be maintained between the barrier and the bumper beam at the position where it is attached to the rear frame. By maintaining the clearance, the timing at which the barrier contacts the collision-side frame would be delayed, and the load can still be transferred to the non-collision-side frame.

FIGURE 12 Schematic diagram of load paths with conventional vehicle in 301

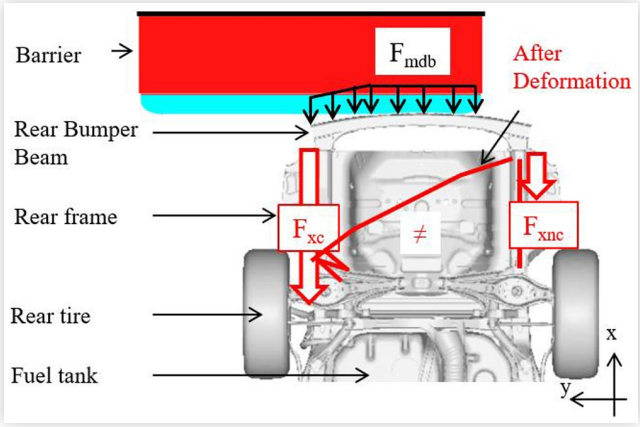

FIGURE 13 New concept for symmetrical load input to the two frames

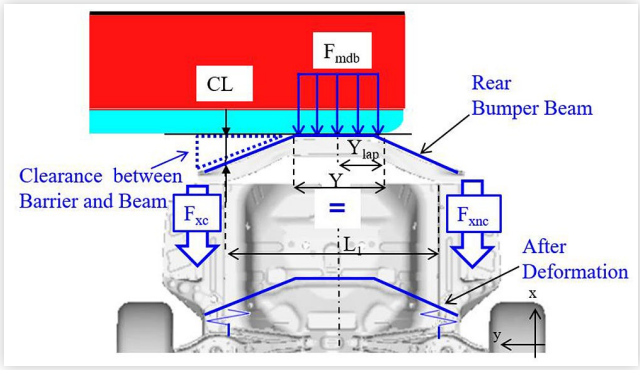

Investigation of Flat Section

Initially, the proposition regarding the flat section of the bumper beam stated in Hypothesis 1 was studied. As shown in Fig. 13, the length from the center of the beam to the end of a contact area with the barrier was defined as Y_{lap}, the length of the flat section of the beam as Y, and the distance between the two rear-frames as L_1. The rear bumper beam was assumed to be a simple beam, and the relationship between Y, F_{xc}, and F_{xnc} was theoretically calculated using the load equilibrium equations (1) and (3) and the moment equilibrium equations (2) and (4). Y_{lap} was set at 250 mm, which is similar to the condition with C-Segment vehicle.

When Y< 2Ylap

$$F_{Xc} + F_{Xnc} = F_{mdb}Y \tag{1}$$

$$\int_{\frac{L_1-Y}{2}}^{\frac{L_1+Y}{2}} F_{mdb}\,y\,dy - F_{xnc}L_1 = 0 \tag{2}$$

When Y≥2Ylap

$$F_{Xc} + F_{Xnc} = F_{mdb}\left(Y_{lap} + \frac{Y}{2}\right) \tag{3}$$

$$\int_{\frac{L_1 - Y}{2}}^{\frac{L_1}{2}+Y_{lap}} F_{mdb}\, y dy - F_{xnc} L_1 = 0 \tag{4}$$

Figure 14 shows the results of the theoretical calculations. The horizontal axis shows the flat section length *Y*, and the vertical axis shows F_{xnc}/F_{xc}. When $Y \leq 500$ mm, the contact area with the barrier is symmetrical with respect to the center of the bumper beam. Therefore, the load transferred from the beam to the two frames is equivalent and hence F_{xnc}/F_{xc}=1.0.

On the other hand, when $Y > 500$ mm, the area of contact is not symmetrical, and the load transferred to the two frames is no longer equivalent. Based on this, to achieve equivalent load distribution to the two frames, it is necessary for *Y* to be equivalent to or less than two times Y_{lap}. Further studies were conducted with *Y* set at 500 mm.

Investigation of Clearance

Next, the proposition regarding the clearance in Hypothesis 2 was studied. For this study, simulation was conducted to determine the influence of timing at which the barrier contacts the bumper beam at the position where it is attached to the rear frame. Figure 15(a) shows a rigid model of the rear bumper beam with the geometry set at *Y*=500 mm and Y_{lap}=250 mm. Length of the initial clearance *CL* was varied by changing the bending angle θ. Based on the mass-production bumper beam, a bending angle of 10° was used as the initial condition, and the angle was increased at 10°intervals up to 60°, as shown in Table 2. *CL* shown in Table 2 was defined as the length between the barrier and the point where the rearmost end of the rear frame and inner ridgeline of the bumper beam cross. Figure 15(b) shows the overall setup for the simulation, including the barrier and the rigid bumper beam. For the simulation, LS-DYNA was used as the solver.

FIGURE 14 Results of theoretical calculations needed for flat section length

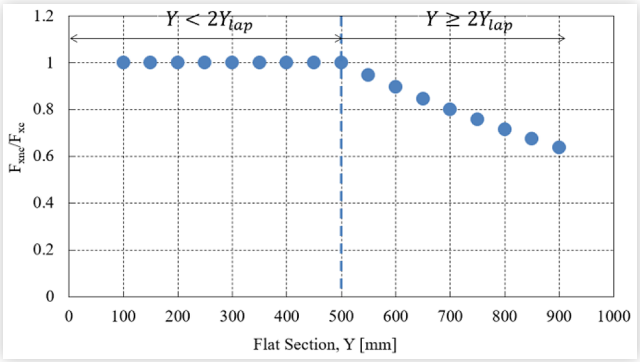

FIGURE 15 A rigid model of rear bumper beam and set up for simulation

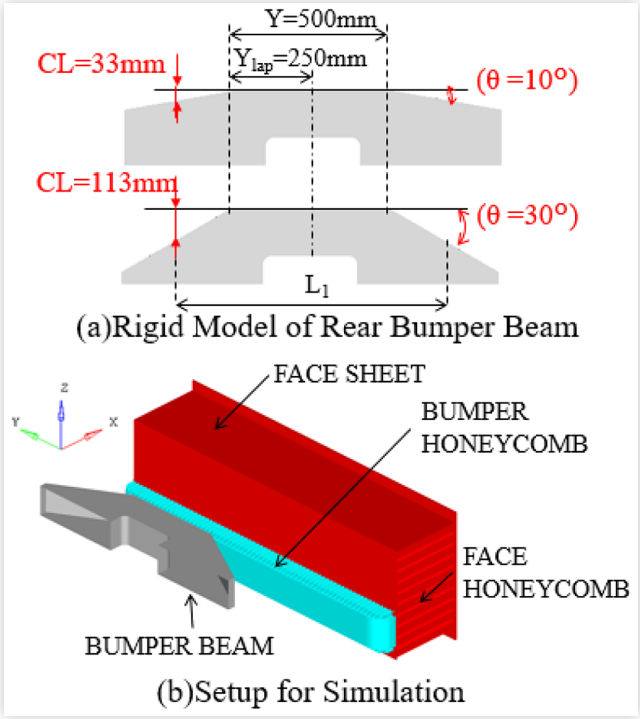

TABLE 2 Simulation conditions for clearance investigation

	CAE01	CAE02	CAE03	CAE04	CAE05	CAE06
Solver	LS-DYNA					
Type	214 Barrier					
I	Rigid					
θ	10°	20°	30°	40°	50°	60°
CL	33 mm	72 mm	113 mm	168 mm	240 mm	346 mm

Simulation Results of Clearance Effect

Figure 16 shows the deformation mode from the simulation results with different *CL*. The results show that as *CL* increases, the contact area with the barrier decreases. In addition, the inflection points on the barrier were found, which are shown as blue points in Fig. 16. Δx, which is the distance in the X direction between the inflection points and the flat section of the beam, was 105 mm irrespective of *CL*.

Figure 17 shows the relationship between F_{xnc} and F_{xc} obtained from the simulation. The black dotted lines indicate the position where F_{xc} is equivalent to F_{xnc}. The results were classified into two groups depending on the bending angle. Fig. 16 (a) shows Group 1, which are the results with $\theta < 40°$; and Fig. 16 (b) shows Group 2, which are for $\theta \geq 40°$. The effect of θ, or *CL* was observed in Group 1, while it had no sensitivity in Group 2 for the load distribution to the collision and the non-collision-side frames.

Figure 18 shows the relationship between the initial clearance *CL* and the load ratio between the two rear frames. The load ratio was enhanced up to *CL*=168 mm, and then saturated

FIGURE 16 Deformation mode from simulation results with different CL

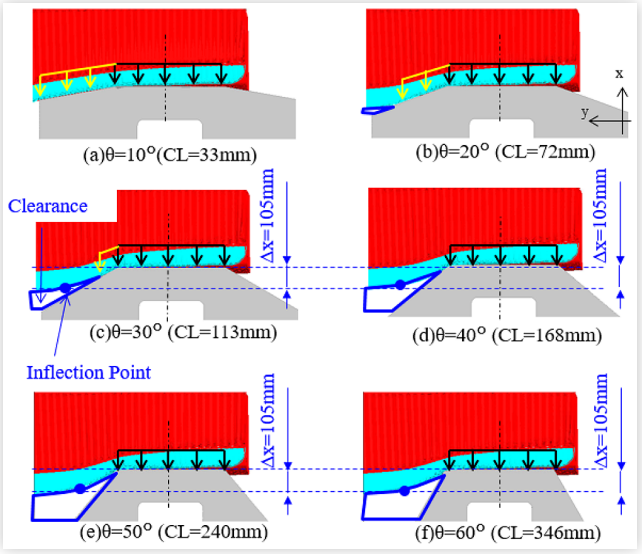

FIGURE 17 Relationship between F_{xnc} and F_{xc} from the simulation results

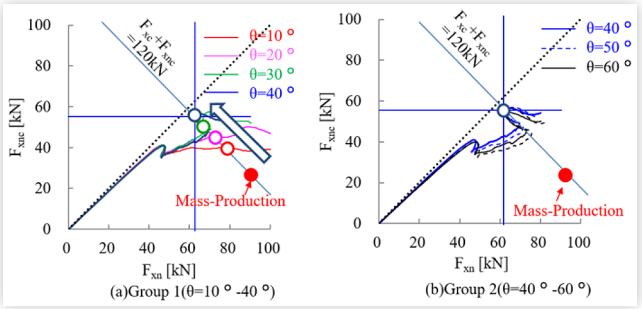

at about 0.9. If *CL* was larger than 105 mm, which corresponds to Δx in Fig. 16, the load ratio would be higher than 0.85, as the inflection point on the barrier would never contact the bumper beam and the contact area would remain on or close to its flat section. From these results, the initial clearance *CL* necessary for the symmetrical load input to the two frames can be defined as $\Delta x \leq CL$, and the beam can distribute the load equally to the two rear-frames.

Feasibility Study of Beam Design

To utilize the results obtained thus far for the actual vehicle application, the beam design parameters were investigated under the restrictions of vehicle design space and manufacturability. Figure 19 shows an example of design space for the rear bumper beam based on the mass-production vehicle. The red dotted line indicates the bumper fascia, and bumper beams with bending angles 20° and 30° are positioned in the design space. If the bending angle θ is 30° or greater to retain sufficient *CL*, it would exceed the design space. The vehicle overhang could be extended in order to secure the design

FIGURE 18 Relationship between F_{xnc}/F_{xc}

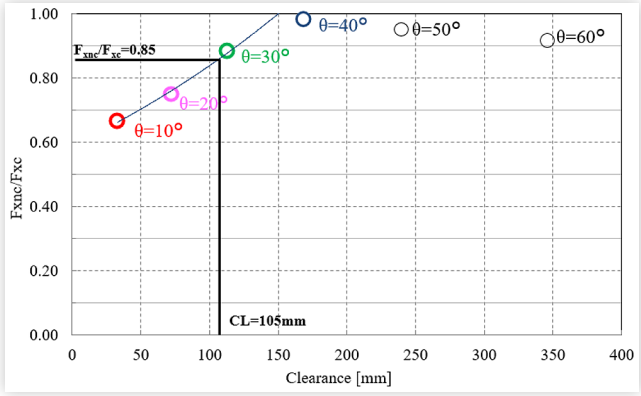

FIGURE 19 Example of design space for mass-production vehicle

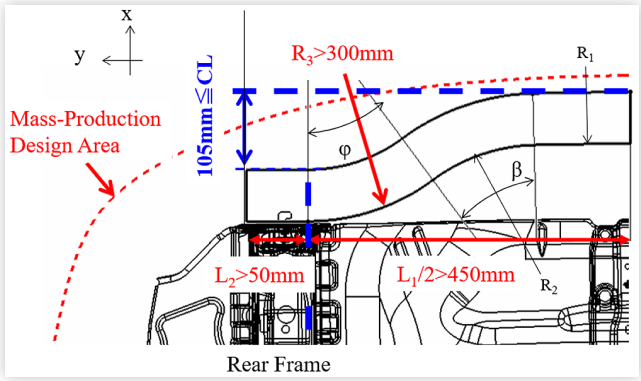

space, but this would have a considerable impact on versatility and the design itself. Thus, to satisfy both the design space and the initial clearance greater than 115 mm as specified in the preceding section, a beam with a two-stage curvature design shown in Fig. 20 was investigated.

For this investigation, the stretch-bending method [11] using aluminum extrusion was applied to manufacture a curvature bumper beam. In this manufacturing method, sagging or local buckling occurs depending on the geometry. As a first step, theoretical calculations were conducted to determine the manufacturable geometry that fits in the design space. For the calculation, two of the geometrical parameters shown in Fig. 20 were applied limitations from the manufacturability restrictions, namely R_3, and L_1. It is necessary for the length of R_3 to be 300 mm or greater, and for the length of $L_1/2$ to be 450 mm or greater. The distance between the two rear-frames is also fixed in the vehicle, which was defined as 1,100 mm for this study. In addition, it is necessary to secure the straight parts larger than 50 mm as mounting points to the rear frames on both sides of the beam, shown as L_2 in Fig. 20. The upper limit therefore for $L_1/2$ would be (1100-2x50)/2=500 mm. Considering these restrictions, the outline of the feasible beam was estimated by varying the bending radius R_2, R_3, the beam length $L_1/2$, and the bending angle β. Since R_1 would be close to linear shape due to its large radius, it was assumed to be flat for this calculation. Figure 21 shows

the results for the feasible outlines that are manufacturable within a mass-production design space. The horizontal axis shows R_3, the vertical axis shows $L_1/2$, and the feasible design area is shown as a rectangle. The upper and lower limits for the bending radius that can be formed at β= 30° and 40° are shown by numbers 1 to 6. These outlines are shown in Figs. 22(a), (b) and (c). Rigid rear bumper models with these shapes were simulated with the same conditions described in the preceding section.

Simulation Results of Stretch-bending Design

Figure 23 shows the relationship between F_{xnc} and F_{xc} obtained from the simulation. For comparison, the black line shows the result for the bending angle θ = 40° (CL = 168 mm) from the preceding section. The waveforms basically indicate the same tendency as the θ = 40° case. Fig. 24 shows the results of the six beams added to Fig. 17. The load ratio F_{xnc}/F_{xc} for all six cases lies close to the θ = 30° case, all of which have a value higher than 0.85. Therefore, CL of 105 mm or more would also be desirable to achieve the load ratio of 0.85 or above for this type of bumper beam. A symmetrical load input to the two rear-frames can still be achieved with stretch-bend-type bumper beam by retaining an initial clearance greater than 105 mm.

FIGURE 20 Geometrical parameters for stretch-bending of bumper beam

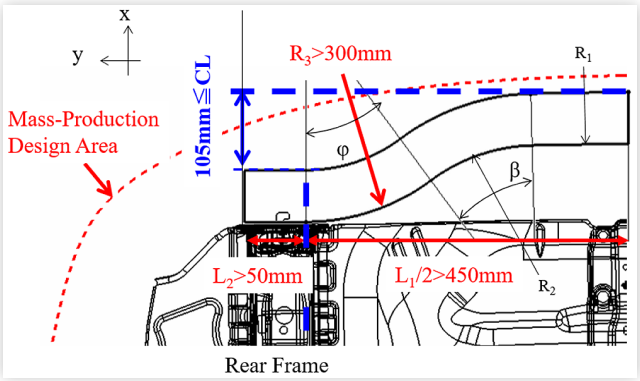

FIGURE 21 Results of feasibility study on manufacturable outline and design space

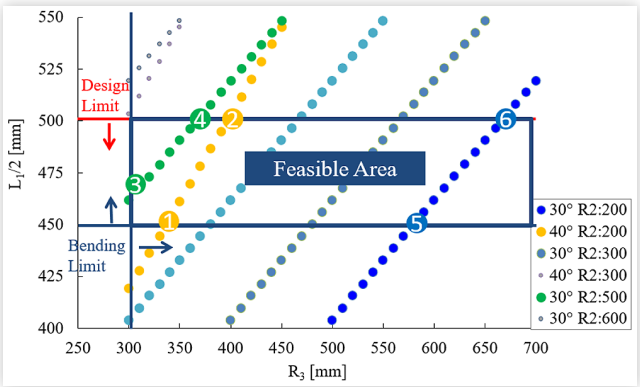

FIGURE 22 Outlines of feasible beam geometries used for simulation

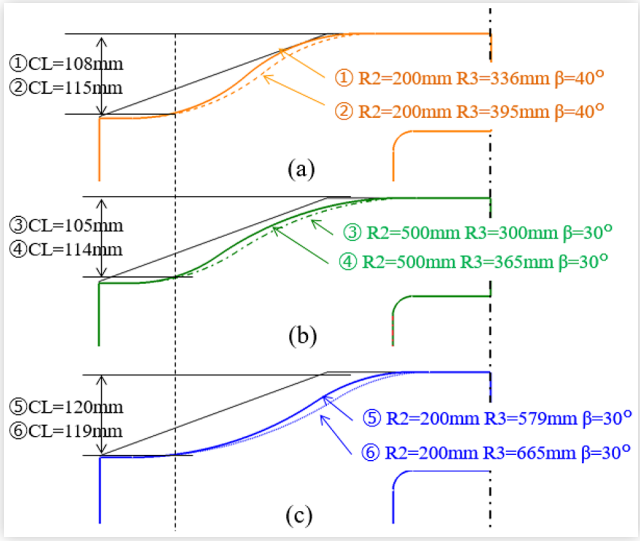

FIGURE 23 Load relationship for stretch-bend bumper outline

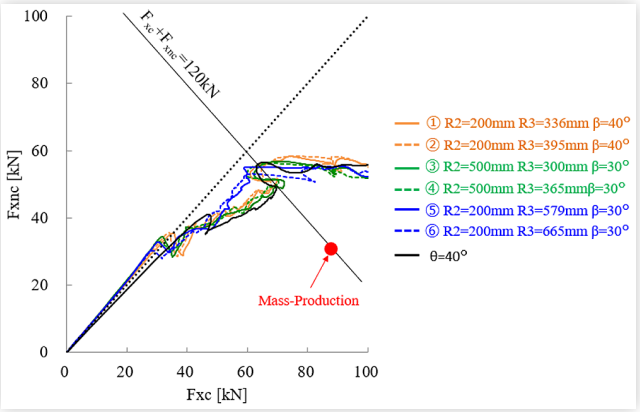

FIGURE 24 Comparison of clearance effect for conventional outline and stretch-bend outline of bumper beam

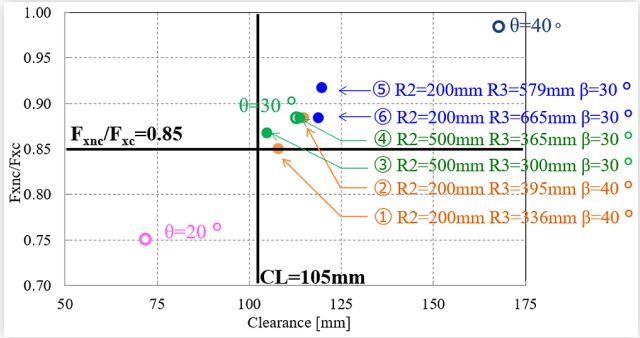

Drop Tower Test

To verify the performance of the bumper beam and the rear frames under the FMVSS 301 test conditions, drop tower tests were performed.

Test Configuration

The testing components were fixed on a flat plate, and a 301 barrier was attached to the drop weight. The barrier was freely dropped in a vertical direction. Two types of tests were conducted, one with a bumper beam only, and the other with a rear floor component. In both cases, a high-speed camera was employed to verify the deformation of the barrier, the bumper, and the rear frames. In addition, target marks (yellow and black circles) were employed to measure the deformation during the test. An accelerometer was attached to the drop weight to measure the dynamic distance that the barrier moved.

Setup for Bumper Beam Test

This test was conducted to verify that the newly developed bumper beam can achieve the symmetrical load input to the two frames. Figure 25 shows the test setup. The bumper beam was fixed to the jigs, and two load cells were positioned below them to measure the load input to both collision- and non-collision-side frames. Two types of bumper beams were tested: A mass-production bumper beam (Test-BPR-01) and a prototype beam (Test-BPR-02). The prototype was designed based on beam number 1 from the previous section, which had the geometry closest to the bending limit for the stretch-bend forming.

Setup for Rear Structure Component Test

This test was conducted to evaluate the load dispersion capability of the prototype component, which includes the newly developed bumper beam and the rear frames proposed in this study. Figures 26 and 27 show the test setup. Test components were fixed to the jigs, and the load cells were positioned in a same manner as in the previous test. Two types of design configuration were tested: One based on a mass-production vehicle (Test-COMPONENT-01) and the other was based on the same vehicle floor but with a prototype bumper beam and prototype rear-frames with four SZs (Test-COMPONENT-02). The SZs are colored yellow in Fig. 26(a) and green in Fig. 26(b). As the results from the previous section suggest that peak load applied to the collision-side frame decreases, the thickness of the rear frame was reduced for the prototype component.

Test Results and Discussion

The performance of the rear bumper beam and the rear structure components were evaluated from the drop tower test results.

FIGURE 25 Test setup for rear bumper beam

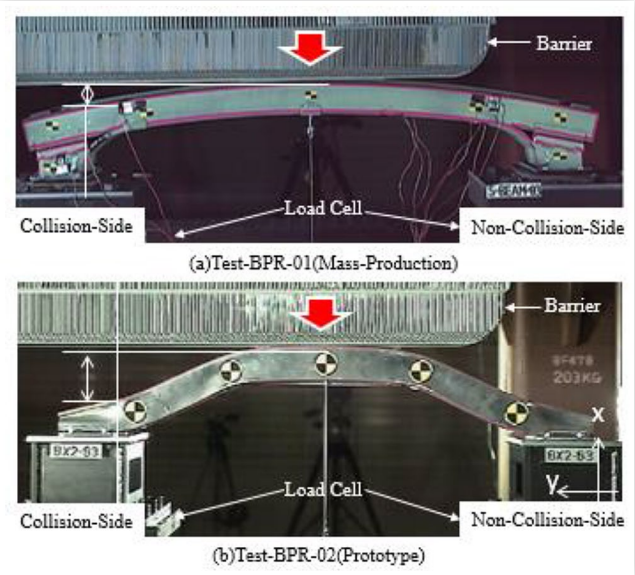

FIGURE 26 Test set up for rear components of mass-production model (Test-COMPONENT-01)

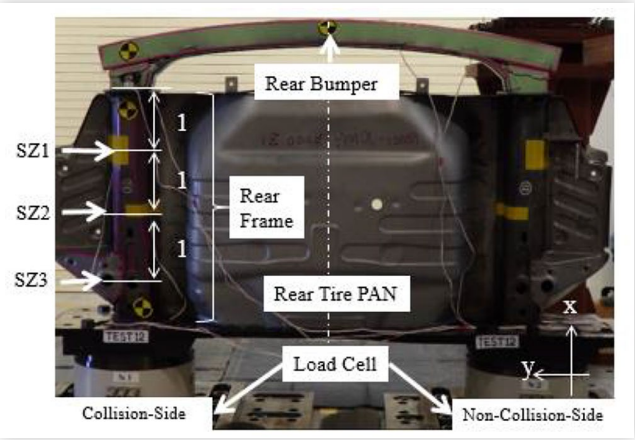

FIGURE 27 Test set up for rear components of new concept (Test-COMPONENT-02)

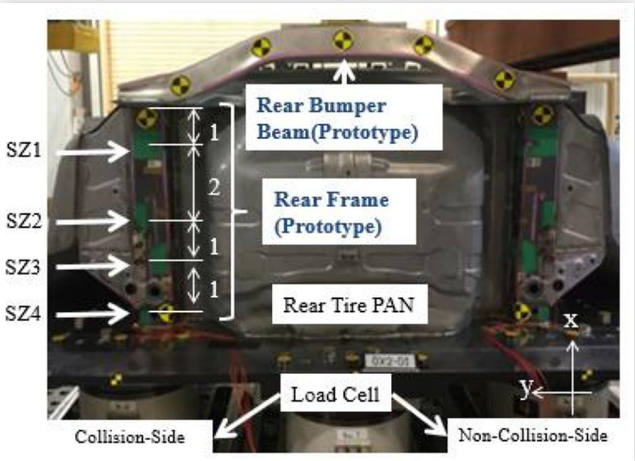

Results of Rear Bumper Beam Test

Figure 28 shows the deformation of the barrier and contact area of the beam during the test. The results indicate that the prototype bumper beam maintained the clearance indicated by the blue circle to delay the contact timing with the barrier. Figure 29 compares the load measured on the mass-production beam and the prototype beams. Points where total load from the barrier reached 120 kN are shown for both the mass-production bumper beam and the prototypes by the red circle and the blue circle, respectively. While there were 50-kN differences in the load input to the two load cells for the mass-production bumper beam, there was only a 4-kN difference for the prototype. The load ratio of 0.93 was achieved with the prototype beam. In addition, the test and the simulation waveforms for the prototype bumper beam were also similar. These results verify that it is possible to achieve symmetrical load inputs and it can be managed with the beam design.

Results of Collision side of Component Test

Figure 30(a) shows a comparison of load measured on the collision-side rear-frame. The deformation ratio (deformation/maximum deformation) is shown on the horizontal axis and the load ratio (load/initial peak load) is shown on the vertical axis. Deformation was calculated from the distance that the target mark attached to the beam had moved in the x direction by commercial image analysis software. The load F was measured by the load cell positioned at the front-end of the rear frame. The results show that the load had dropped after the first peak for the COMPONENT-01, which had three SZs, but for the COMPONENT-02 with four SZs, the load had recovered after the drop from the first peak and repeated similar behavior thereafter, as indicated by circled numbers 1 to 3. Figure 30(b) shows a comparison of average load during the deformation. COMPONENT-02 was approximately 1.8 times higher than the other. The difference from the simulation model A' was only 7%.

Figures 31(a) and (b) show the deformation mode in series for both components: I is prior to the deformation; II is the initial deformation; III is at the middle of the deformation; and IV at is the end of the deformation. In COMPONENT-01, deformation had started from SZ1 and 2. At timing III, the rear frame started to tilt, and the centerline of the frame moved from the white-dotted line to the yellow-dotted line. This is believed to the reason that the load was not recovered after the first peak and the average load remained low. For COMPONENT-02, the deformation had started from SZ1 by crushing. At timing III, SZ2 and 3 had started to deform as bending initiation points, and the centerline of the frame remained closer to the white dotted line until timing IV. This deformation generated a similar effect as an axial crushing of the frame and brought on the load recovery during the crash duration. These results verify that it is possible to increase the energy absorption efficiency by optimizing the number of bending points and the positioning of the SZ.

FIGURE 28 Deformation of the barrier and contact area of bumper beam

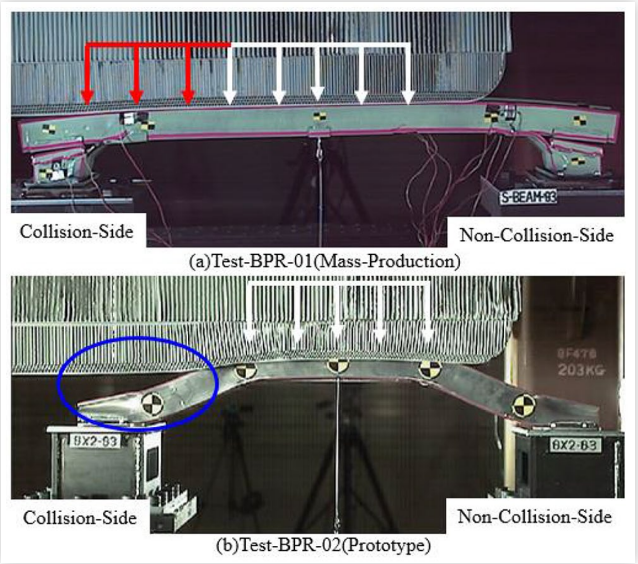

FIGURE 29 Comparison of test results with mass-production and prototype beams

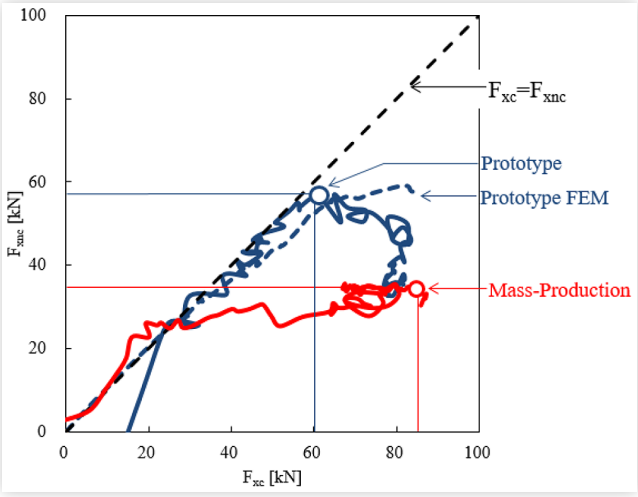

FIGURE 30 Comparison of load with mass-production and new concept

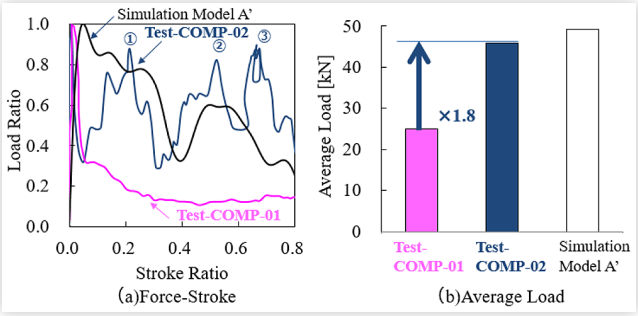

FIGURE 31 Deformation mode in series for mass-production and new concept

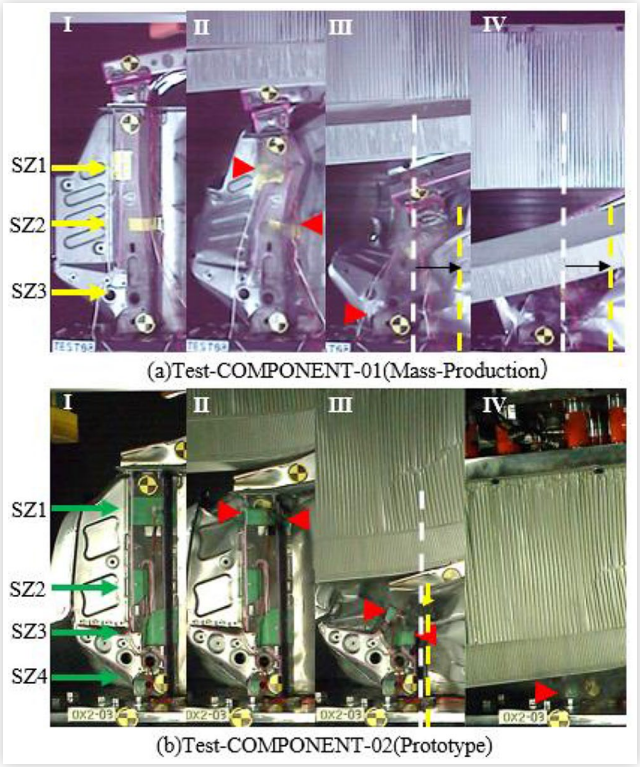

Results of Non-Collision-side of Component Test

Figure 32 shows a comparison of the deformation mode of the component including the non-collision-side frame. The results for COMPONENT-02 show that the effect of the bumper beam resulted in an increase in the deformation of the non-collision-side frame.

Figure 33 shows a comparison of the load-stroke curves between the collision- and the non-collision-side frames. Fig. 33(a) shows the mass-production component and Fig. 33 (b) shows the prototype. The solid lines in Fig. 33 show the collision-side frame, and the dotted lines show the non-collision-side frame. A symmetrical load input to the two frames was observed in the prototype component. Figure 34 shows the energy absorption calculated by an integration of the load-stroke curves at the deformation, in which the beam was

FIGURE 32 Comparison of deformation mode of non-collision-side frame

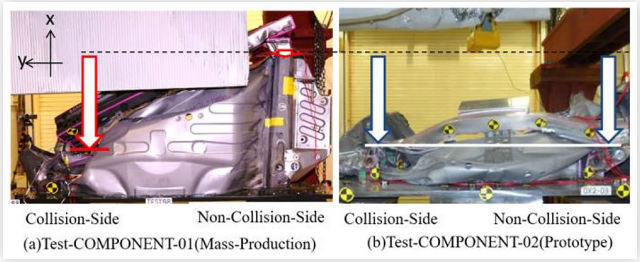

FIGURE 33 Comparison of load-stroke curves of collision- and non-collision-side frames

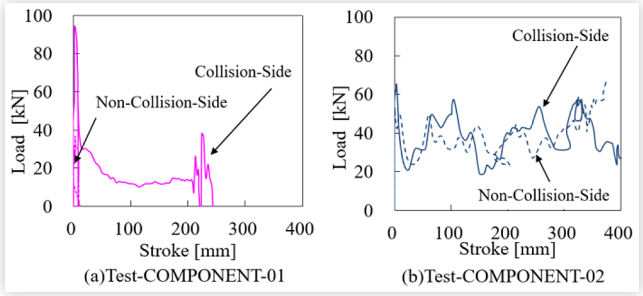

FIGURE 34 Comparison of energy absorption

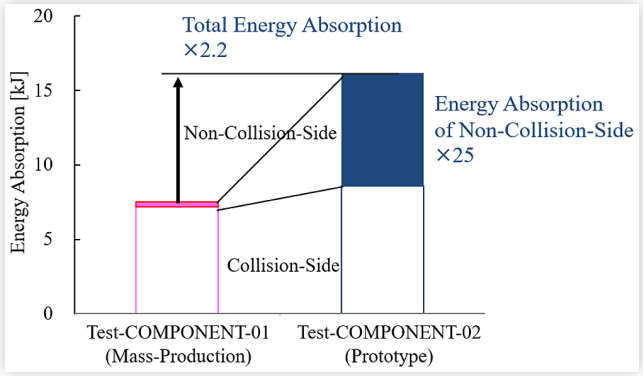

stroked 250 mm. The energy absorption of the non-collision-side frame was 7.6 kJ in the prototype, which was approximately 25 times higher than the mass-production component. In terms of the total energy absorption by the components, the new concept achieved 2.2 times higher absorption than the mass-production component.

Weight Reduction Effect

Based on the test results in the previous section, additional study was conducted regarding the potential weight savings in the rear frame. Figure 35 shows the one-dimensional (1D) model used in this study. The 1D model was mainly composed of two sets of spring elements, one on the barrier and the other on the vehicle. The spring element on the vehicle was further divided into two frames, floor panel, cabin, and other parts such as tires and suspensions, and they were connected in parallel. The springs of the rear frames were divided into three sections A, B, and C, as shown Fig. 35. With the new concept, the rear bumper distributes the load equivalently to the collision- and the non-collision-side frames. From Fig. 34, the new concept was able to absorb approximately 2.2 times higher energy than the mass-production structure. From the 1D model analysis, the peak load necessary for rear frame A could be reduced by 17% against the mass-production model, with no additional deformation on the body. The study with the 1D model estimated 17% weight reduction of

rear frame A by changing the thickness, without changing shape or materials.

Figure 36 shows a comparison of the full-vehicle simulation results between the mass-production structure and the new concept with additional 17% weight reduction of rear frame A. The simulation verified that it was possible to deform the non-collision-side frame in the same way as in the drop tower test. Figure 37(a) shows the energy absorption and the average load for the two frames, and (b) shows the deformation of the vehicle body indicated as "Deformation" in Fig. 36. Figure 37(a) indicates an increase of approximately 1800% in energy absorption by the non-collision-side frame and of approximately 210% by the rear frame in total. Fig. 37(b) shows the degree of deformation is equivalent to or lower than that of the mass-production vehicle. These results indicate that the proposed configuration is able to reduce the weight of the rear frame.

FIGURE 35 1D model and calculated load profile for mass-production and new concept

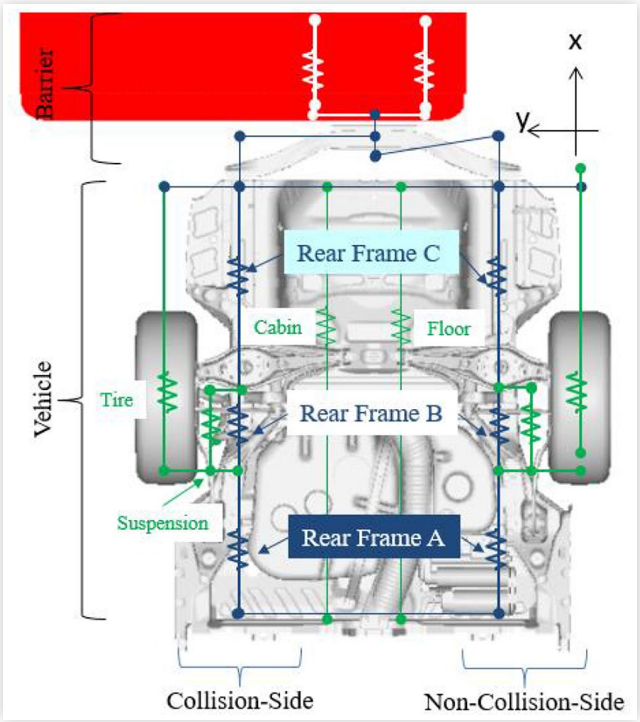

FIGURE 36 Comparison of full-car simulation results of mass-production and new concept

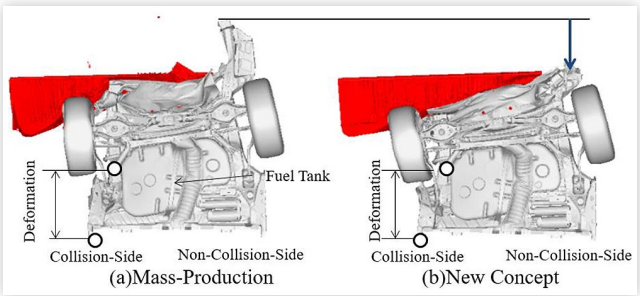

FIGURE 37 Comparison of energy absorption and deformation of mass-production and new concept from simulation

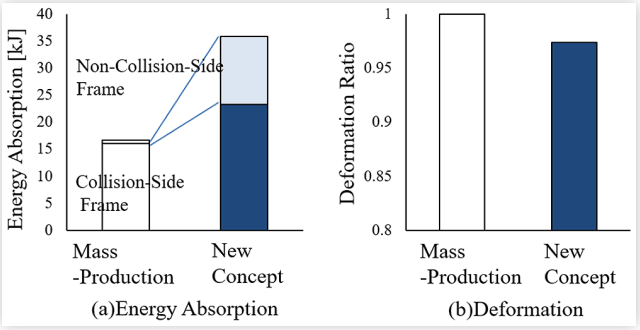

Conclusions

The new concept applied to the rear frames and the rear bumper beam showed the capabilities of increasing the energy absorption efficiency in FMVSS 301 and of potential weight reduction.

The technological details of this research are summarized as follows:

1. The relationship between the number of bending points, the positioning of the soft-zones and the energy absorption performance in the rear frame was clarified.
2. Geometrical conditions of the bumper beam to achieve symmetrical load input to the two rear-frames were clarified. By applying a symmetrical load input, it is possible to increase the energy absorption on the non-collision-side frame.
3. The findings described in the two points above were verified by drop tower tests.

The rear body configuration discussed in this paper is able to increase the energy absorption efficiency of the vehicle and can be expected to be an effective technology for a next-generation vehicle, against the background of concerns that electrification will increase vehicle weight.

References

1. U.S. Department of Transportation National Highway Traffic Safety Administration, "Laboratory Test Procedure for FMVSS 301R Fuel System Integrity - Rear Impact," TP-301R-02, January 17, 2007.
2. Emura, M., Takizawa, S., Higuchi, E. et al., "Research on Compatibility in Car-to-Car Side Impacts," *Transactions of Society of Automotive Engneers of Japan* 38(6):289-295, 2007.
3. Motozawa, Y., Yamaki, J., Abe, T. et al., "Fundamental Study on the Seat Integrated Load-Path Structure for Side Impacts," *JSAE Journal* 44(1):125-130, 2013.
4. Motozawa, Y., Urushiyama, Y., and Yamaki, J., "Fundamental Study on the High-Strength Body Structure Oriented to the Enhancement of the Ride Down Effect during Vehicular Side Impact," *JSAE Journal* 43(1):21-26, 2012.

5. Ishitobi, H. and Fujiwara, A., "Deformation of Aluminum Bumper Beam in Corner Pendulum Impact Test," *JSAE Journal* 29(2):97-102, 1998.
6. Yabu, T. and Yasuhara, S., "Development of Rear Bumper Beam Using Thermoplastic Glass Fiber-Reinforced Plastic," *Honda Technical Review e-Book* 30(1), 2018.
7. Yasuyama, M., "Resistance Spot Welding of Hot Stamp Steel Sheets," *Journal of the Japan Welding Society* 84(6):447-451, 2015.
8. Fukuchi, H. and Nomura, N., "Automotive Solution: Development of Hot Stamping with High Productivity," *Shinnittetsu giho* (402):70-72, 2015.
9. Maki, H. and Takaki, N., "Application of Next-Generation High-Lambda-Type High-Strength Steel Sheets," *JSAE Journal* 48(6):1347-1352, 2017.
10. Uchihara, M., Fukui, K., "The Performance of Tailor Welded Blanks Using High Strength Steel Sheets for Practical Use: The Study of Tailor Welded Blanks Using Automotive High Strength Steel Sheets: Report 2," *Journal of the Japan Welding Society*, 23(4), 549-557, 2005-11-05
11. Paulsen, F. and Welo, T., "A Design Method for Prediction of Dimensions of Rectangular Hollow Sections Formed in Stretch Bending," *Journal of Materials Processing Technology* 128:48-66, 2002.

Contact Information

Atsushi Hasegawa
Honda R&D Co., Ltd. Automobile R&D Center
4630 Shimotakanezawa, Haga-machi, Haga-gun,
Tochigi 321-3393, Japan
Atsushi_Hasegawa @n.t.rd.honda.co.jp

Definitions/Abbreviations

1D - one dimensional

301 - North American rear collisions safety requirement FMVSS 301

CL - length of initial clearance between the barrier surface and a point on the bumper beam surface at which the rear frame is attached

FEM - finite element method

HZ - hard zone

SZ - soft zone

TZ - transition zone between hard zone and soft zone

collision-side frame - A rear-frame that directly collide with the barrier

non-collision-side frame - A rear-frame that does not directly collide with the barrier

F - load

F_{mdb} - distributed load applied from barrier to bumper beam

F_{xc} - load input from bumper beam to collision-side frame

F_{xnc} - load input from bumper beam to non-collision-side frame

L_1 - distance between two rear frames

L_2 - length of straight part of bumper beam ends

R_2 - bending radius of bumper beam (applied for stretch beniding)

R_3 - bending radius of bumper beam (applied for stretch beniding)

Y - flat section length of bumper beam

Y_{lap} - length from center of bumper beam to end of contact area with barrier

Δx - distance in X direction between inflection point and flat section of bumper beam

β - bending angle of bumper beam (applied for stretch bending)

Φ - bending angle of bumper beam (applied for stretch bending)

θ - bending angle of bumper beam

ISSN 0148-7191